PHYSICAL REVIEW C VOLUME 47, NUMBER 1 JANUARY 1993

Short lifetimes in ^{28}Si

P. Tikkanen, J. Keinonen, and A. Kangasmäki
Accelerator Laboratory, University of Helsinki, Hämeentie 100, SF-00550 Helsinki, Finland

Zs. Fülöp, Á. Z. Kiss, and E. Somorjai
Institute of Nuclear Research of the Hungarian Academy of Sciences, H-4001 Debrecen P.O. Box 51, Hungary
(Received 18 August 1992)

Mean lifetimes of levels in ^{28}Si have been measured using the Doppler-shift-attenuation (DSA) method in conjunction with the reactions ^{14}N(^{16}O,pn)^{28}Si and ^{27}Al(p,γ)^{28}Si. The lifetime values were determined for 16 bound levels below the excitation energy of 10 MeV and for the 10.42-, 10.67-, 11.10-, and 11.51-MeV alpha unstable states, and the 12.99-MeV proton or alpha unbound state. The lifetimes of the three last levels are reported for the first time. The targets were prepared by implanting ^{14}N into Ta, and ^{27}Al into Ta and Si substrates. The experimental stopping power of Ta for Si ions was determined by application of the inverted analysis of DSA data from the reaction ^{2}H(^{28}Si,$p\gamma$)^{29}Si. Computer simulations with the Monte Carlo method and experimental stopping power were used in the DSA analysis. Experimental transition matrix elements, based on the measured mean lifetime values, are compared with predictions of the universal *sd*-shell model.

PACS number(s): 21.10.Tg, 27.30.+t

I. INTRODUCTION

The nucleus ^{28}Si is one of the most interesting and most studied nuclei in the *sd*-shell region. Since ^{28}Si is in the middle of the *sd* shell, it can be described as having either 12 particles or 12 holes in this shell, and thus represents a challenge for nuclear models. The experimental spectrum of ^{28}Si has recently been shown to be reproduced quite well with the universal *sd*-shell (USD) model [1]. The USD calculations have been carried out for all $8 \leq N, Z \leq 20$ systems in the complete space of $0d_{5/2}$-$1s_{1/2}$-$0d_{3/2}$ basis vectors [2–4]. The Hartree-Fock calculations [5] as well as the Nilsson-Strutinski cranking formalism [6, 7] predict the experimentally established oblate ground state deformation for ^{28}Si [8], and a number of excited prolate and oblate bands which have also been observed experimentally [1]. Both kinds of bands have been shown to be reproduced in the USD model calculations as well [1, 9].

In the present work, accurate mean lifetimes of states in ^{28}Si have been obtained for the deduction of experimental electromagnetic transition matrix elements, mainly $E2$ matrix elements, and their comparison with the matrix elements deduced from the shell-model wave functions. The present work is a continuation of our systematic study of the short lifetimes in the *sd*-shell nuclei using the improved Doppler-shift-attenuation (DSA) method as developed at the Helsinki University Accelerator Laboratory [10–16].

Several studies [17, 18] have been reported in the literature on the lifetime values of states in ^{28}Si previous to this experiment. The most extensive studies are based on the capture reaction ^{27}Al(p,γ)^{28}Si. The previously existing information on lifetimes was mainly obtained in low-recoil-velocity DSA measurements with the ^{27}Al(p,γ)^{28}Si and ^{25}Mg(α,n)^{28}Si reactions [17,18]. High-recoil-velocity lifetime measurements have been performed only for the first excited state through the reaction ^{4}He(^{28}Si,α')^{28}Si [18]. Because a variety of evaporated targets with low stopping powers were used in most DSA measurements of short lifetimes and because the slowing-down theory [19] was used in many instances without sufficient experimental confirmation, the reported values have large uncertainties and mutual inconsistencies.

In the DSA measurements of the current work, the heavy-ion reaction ^{14}N(^{16}O,pn)^{28}Si and the capture reaction ^{27}Al(p,γ)^{28}Si have been employed. This work is the first study on short lifetimes ($\tau < 1$ ps) for the high-lying excited states where heavy-ion-induced reactions and high recoil velocities have been utilized. The effective stopping power is obtained by using implanted ^{14}N and ^{27}Al targets in Ta. In order to get a more accurate value for the long lifetime ($\tau \geq 1$ ps) of the 6.28-MeV state, implanted targets in Si are also used. In comparison with the previous lifetime measurements the use of implanted targets is an essential advantage in the determination of short nuclear lifetimes with the DSA method. Additional advantages are the use of the experimentally known stopping power, the computer simulation of γ-ray line shapes with the Monte Carlo (MC) method, and the consistent use of the same technique in the DSA analysis of the high-recoil-velocity [the reaction ^{14}N(^{16}O,pn)^{28}Si] and low-recoil-velocity data [the reaction ^{27}Al(p,γ)^{28}Si]. The present technique allows sufficiently accurate determination of mean lifetime values, in order to extract $M1$ and $E2$ transition matrix elements for a meaningful test of the USD shell model.

II. EXPERIMENTAL ARRANGEMENTS

In the ^{14}N(^{16}O,pn)^{28}Si reaction studies, 20–28 MeV ^{16}O beams of about 200 particle nA were supplied by the 5-MV tandem accelerator EGP-10-II of the Helsinki University Accelerator Laboratory. The beam spots were 2×2 mm^2 on the target. In the ^{27}Al(p,γ)^{28}Si reaction studies, the 5-MV Van de Graaff accelerator of the Institute of Nuclear Research in Debrecen supplied 0.66–1.32-MeV proton beams of about 13 μA for measurements with Ta backing and 3 μA with Si backing. The beams were collimated to form a spot 5 mm in diameter on the target.

The ^{14}N targets were prepared by implanting a 20 μg cm^{-2} fluence of 100-keV ^{14}N$^+$ ions into 0.4-mm-thick Ta sheets at the isotope separator of the Helsinki University Accelerator Laboratory. The ^{27}Al targets were prepared by implanting a 12 μg cm^{-2} fluence of 60-keV ^{27}Al$^+$ ions into 0.4-mm-thick Ta sheets or into 2-mm-thick high-purity Si wafers at the isotope separator.

The ^{2}H targets for the stopping power measurement via the ^{2}H(^{28}Si,p)^{29}Si reaction were prepared by implanting first 6.0×10^{17} at. cm^{-2} 100-keV ^{20}Ne$^+$, and then 10^{18} at. cm^{-2} 25-keV ^{2}H$^+$ ions into Ta sheets. The ^{20}Ne implantation was necessary in order to provide trapping sites for ^{2}H at the Ne precipitates and thus to avoid the outdiffusion of ^{2}H [20]. The vacancies produced in the ^{2}H implantation migrated to the Ne precipitate Ta interface and then effectively trapped ^{2}H atoms [20, 21]. In order to check the possible effect of the implanted material on the stopping power, the targets implanted with only 6.0×10^{16} ^{20}Ne$^+$ and ^{2}H$^+$ ions cm^{-2} were also used.

During the measurements, the ^{14}N and the ^{2}H targets were set perpendicular relative to the beam. The target holder made of copper was air cooled. A vacuum better than 2 μPa was maintained in the target chamber to prevent carbon buildup. The deposition of carbon was continuously monitored by the use of the strong 1369-keV ^{24}Mg γ-ray peak from the reaction ^{12}C(^{16}O,$\alpha\gamma$)^{24}Mg. The ^{27}Al target was set perpendicular to the beam in a target holder which provided direct water cooling of the Ta sheet and indirect water cooling for the Si backing.

The γ radiation resulting from target bombardment was detected both in the ^{14}N(^{16}O,pn)^{28}Si and in the ^{2}H(^{28}Si, $p\gamma$)^{29}Si reaction measurements by an escape-suppressed spectrometer (ESS), which consisted of an Ortec HPGe detector (with 40% efficiency) surrounded with a cylindrical (thickness 4 cm and length 22 cm) Harshaw bismuth-germanate (BGO) veto detector. The BGO detector was surrounded by a cylindrical 3-cm-thick lead shield. The energy resolution of the spectrometer was 2.0 keV at $E_\gamma = 1.33$ MeV and 2.8 keV at $E_\gamma = 2.61$ MeV. The escape suppression factor was 3–5. In the ^{27}Al(p,γ)^{28}Si reaction measurements, a 25% efficient Ortec HPGe detector without escape suppression was used. The energy resolution of the detection system was 2.2 keV at $E_\gamma = 1.46$ MeV and 3.0 keV at $E_\gamma = 2.61$ MeV. The detector was shielded by a 6-cm-thick lead shield against the laboratory background radiation.

The γ-ray spectra were stored in a 4, 8, or 16 kbyte channel memory with dispersions of 0.29–2.0 keV/channel. The stability of spectrometers was checked with a ^{208}Tl γ-ray source and the ^{40}K laboratory background. The energy and efficiency calibrations of the γ-ray detectors were done with ^{56}Co and ^{66}Ga sources [22] placed in the target position. The stop peaks from the decay of long-lived states were utilized for internal calibration of γ-ray energies.

III. MEASUREMENTS AND RESULTS

A. Stopping power

The stopping power of the slowing-down medium (Ta or Si) for Si ions was described in the DSA analysis according to the following equation:

$$\left(\frac{dE}{dx}\right)_{\rm corr} = f_n \left(\frac{dE}{dx}\right)_n + \left(\frac{dE}{dx}\right)_e^{\rm exp} . \quad (1)$$

The uncorrected nuclear stopping power $(dE/dx)_n$ was calculated by the MC method, where the scattering angles of the recoiling ions were directly derived from the classical scattering integral [10] and the interatomic interaction was described by the universal potential [Ziegler, Biersack, and Littmark (ZBL)] given by Ziegler *et al.* [23]. The correction parameters f_n(Ta) $= 0.70\pm0.05$ and f_n(Si) $= 0.97\pm0.05$ for the nuclear stopping power of polycrystalline Ta and of single-crystal Si, respectively, for Si ions, are based on studies on the nuclear stopping power at low velocities done in the University of Helsinki Accelerator Laboratory [10, 24–26]. The values of the nuclear correction factor f_n, given here relative to the universal potential, are slightly larger than the values reported previously for the Thomas-Fermi potential [f_n(Ta) $= 0.67\pm0.05$, f_n(Si) $= 0.95\pm0.05$ in Refs. [25, 26], respectively].

The electronic stopping power $(dE/dx)_e$ of tantalum for ^{29}Si ions at velocities $v = 0 - 6v_0$ (here $v_0 \approx c/137$ is the Bohr velocity, and c is the velocity of light) was determined by use of the reaction ^{2}H(^{28}Si, $p\gamma$)^{29}Si with ^{28}Si beam energies of 23–33 MeV. The well-established mean lifetime value of the first excited state in ^{29}Si ($\tau = 420 \pm 15$ fs, $E_x = 1273$ keV; Ref. [18]) was used as a standard in the analysis of the line shape of the $1.27 \rightarrow 0$ MeV transition. The uncertainty of the electronic stopping power, shown in Fig. 1 along with the values of Ziegler *et al.* [23], was estimated to be $\pm5\%$. For more details of the stopping power measurements, and for the electronic stopping power of silicon for Si ions, see Ref. [27].

Based on our studies on the effect of implanted target atoms on the density of the backing material and lifetime values obtained by DSA [10, 11, 25] along with the fluences of ^{20}Ne, ^{2}H, ^{14}N, and ^{27}Al, the implanted layers were assumed to have an insignificant effect on the density of Ta or Si probed by $\beta = v/c \approx 0.03$ or 0.002 ^{28}Si recoils or $\beta \approx 0.04$ ^{29}Si recoils. This was further confirmed in the stopping power measurement where no differences within statistical uncertainty were seen between the line shapes obtained with low- and high-fluence ^{2}H targets.

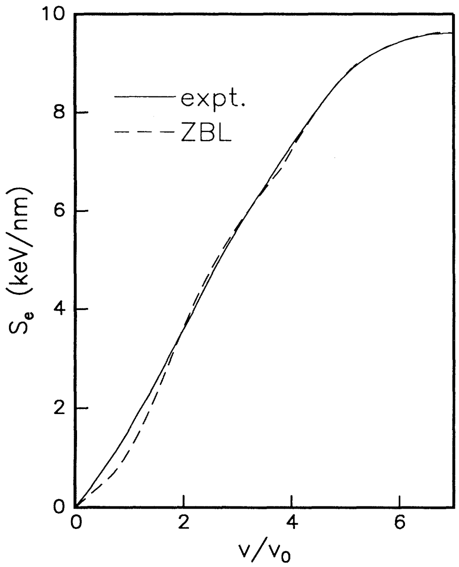

FIG. 1. Experimental (solid line) and empirical (dashed line, Ref. [23]) electronic stopping power (S_e, in keV/nm) of tantalum for ^{29}Si ions as a function of the ion velocity (v, in units of the Bohr velocity v_0).

B. The ^{14}N(^{16}O,pn)^{28}Si reaction study

The Doppler-shifted γ rays were detected at the angle 0° relative to the beam direction. The detector was located 4.0–8.0 cm from the target and an absorber of 2 mm Pb, 1 mm Cd, and 1.5 mm Cu was used between target and the detector front face to reduce the counting rate due to low energy γ rays and x rays. The corrections for solid-angle attenuation of the observed Doppler shifts and for the finite initial velocity distribution were checked from fully shifted γ rays of known short-lived states ($\tau < 10$ fs). The measured dependence of the detector efficiency on the angle between the detector symmetry axis and the direction of γ-ray detection was taken into account.

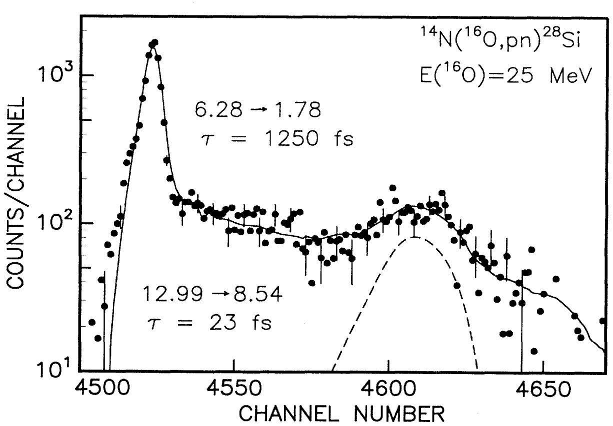

FIG. 2. Portion of background-corrected γ-ray spectrum recorded in the heavy-ion reaction ^{14}N(^{16}O,pn)^{28}Si DSA measurements of the 6.28-MeV (6.28 → 1.78 MeV transition), and the 12.99-MeV (12.99 → 8.54 MeV transition) ^{28}Si states. The dispersion is 1.0 keV/channel. The solid line is the sum of the two simulated line shapes for the shown lifetimes of the states; $\tau(6.28) = 1250\pm150$ fs, and $\tau(12.99) = 23\pm5$ fs. The dashed line is the simulation for the 12.99-MeV state lifetime only.

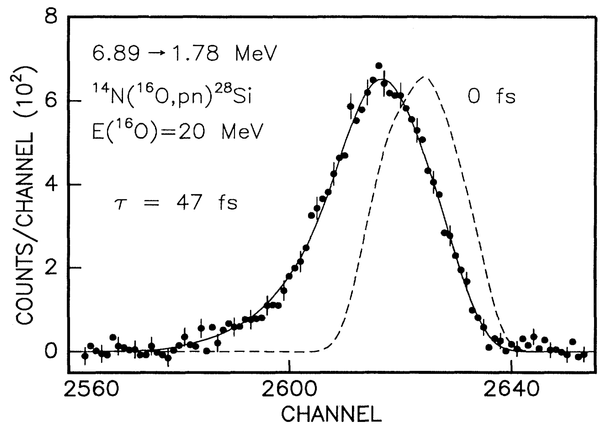

FIG. 3. As for Fig. 2, but for the 6.89-MeV state (6.89 → 1.78 MeV transition). The dispersion is 2 keV/channel. The Monte Carlo simulation is for the lifetime 47 fs. The dashed line is the simulation for a lifetime $\tau = 0$, and illustrates the effects of the reaction kinematics and the finite solid angle of the γ-ray detector.

The energy loss of the ^{16}O beam, ranging from 410 keV (28 MeV) to 430 keV (20 MeV) for an implantation depth of 100 nm Ta, was included in the simulation of the initial velocities of the recoiling ^{28}Si ions.

Figures 2–4 show portions of the γ-ray spectra from the DSA measurements of the 6.28-, 6.89-, and 8.54-MeV states. The DSA analysis was performed by the computer simulation of γ-ray line shapes with the MC method [10–16]. A summary of the results is given in

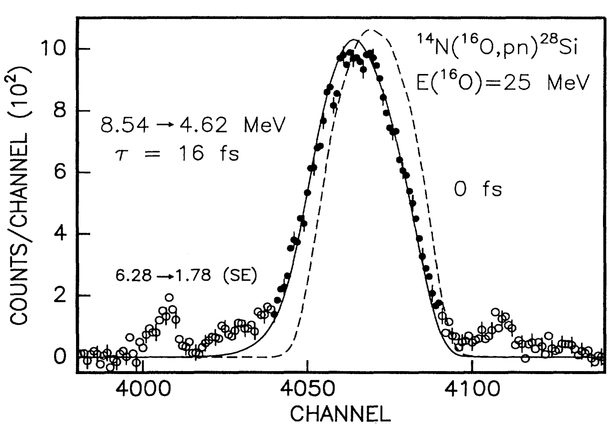

FIG. 4. As for Fig. 3, but for the 8.54-MeV state (8.54 → 4.62 MeV transition); $\tau(8.54) = 16.4\pm1.4$ fs. The dispersion is 1.0 keV/channel. Only the region shown with solid points was included in the line-shape fitting. (SE represents single-escape peak).

Table I. Several γ-ray peaks were included in the DSA analysis for each state when possible.

To control the effect of the feeding transitions on the γ-ray line shapes and deduced lifetime values, the measurements through the reaction $^{14}N(^{16}O,pn)^{28}Si$ were performed at $E(^{16}O)$ = 20, 22, 25, and 28 MeV. In the deduction of the lifetime values from the line shapes, the corrections for indirect feedings were obtained by measuring the population of the ^{28}Si states at each energy of the oxygen beam, and utilizing the γ-ray decay schemes of the states extensively studied in the literature [18].

A simulated line shape was obtained as the sum of the shapes corresponding to the direct prompt and delayed feeding of the state. The sum was weighted by the experimental fractions of the feedings. In the deduction of the lifetime value for the 6.89-MeV state from the data obtained at bombarding energy of 20 MeV, 8.0±1.0 % feeding from the 8.95-MeV state ($\tau = 70 \pm 8$ fs) and 3.0±0.8 % feeding from the 11.51-MeV state (13±3 fs) was used. The corresponding fractions were 9.2±1.1% and 5.0±0.9 % at $E(^{16}O)$ = 25 MeV. The lifetime value of the 8.54-MeV state was corrected for the 7.2±0.9 % feeding from the 12.99-MeV state (23±5 fs) at 25 MeV. The feedings from the 12.99-MeV state to the 11.10-MeV state with fractions of 8.5±1.2 % and 6.0±1.0 % at 25- and 28-MeV bombarding energies, respectively, were taken into account in the analysis.

TABLE I. Summary of the lifetimes in ^{28}Si as obtained in the present work with the $^{14}N(^{16}O,pn)^{28}Si$ reaction.

E_x (MeV)	τ^a (fs) as measured at $E(^{16}O)$ (MeV) 20	22	25	τ^b (fs)
4.98	48±2	45±3	64±5[c]	47±3
6.28			1250±130	1250±150
6.89	46.0±1.0	36±2	51.0±1.0	47±8
7.38	10±2	10±5	13±2	11.5±1.5
7.42	54±3	49±3	67±3[c]	51±4[d]
7.93	18±2	14±2	12±5	16±2
8.54	16±2		16.5±0.7	16.4±1.4
8.95	70±12	70±8		70±8[e]
9.48	<10		7±3	7±3
10.42			38±10	38±10
11.10	13±3		16.5±1.4	15.9±1.5[f]
11.51	10±8	15±4	10±5	13±3
12.99			26±5	23±5[g]

[a]Values given are corrected for the feedings and are based on the line-shape analysis. Only statistical errors are shown.
[b]Weighted average values, which include the 5% uncertainty in the experimental stopping power.
[c]Effective lifetime containing unknown feeding, value rejected in calculation of the weighted average.
[d]Measurement at $E(^{16}O)$=28 MeV yields a lifetime of 58±6 fs which is not included in the average due to the feeding.
[e]Measurements at both $E(^{16}O)$=25 MeV and 28 MeV yield 70 fs if a delayed 20-fs 100% feeding is assumed.
[f]Included also in the average is 15±3 fs obtained at 28-MeV bombarding energy.
[g]The value 20±5 fs obtained at $E(^{16}O)$ = 28 MeV is also taken into account.

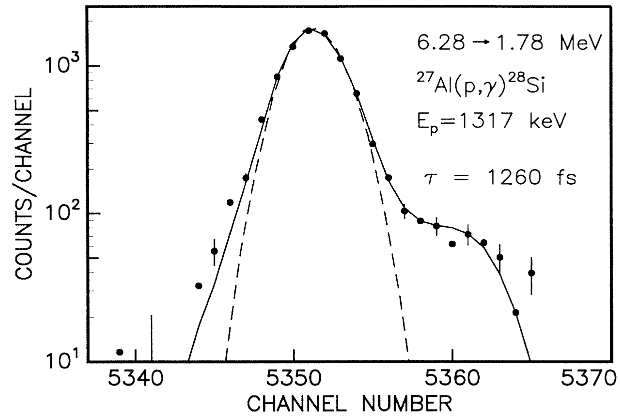

FIG. 5. As for Fig. 3, but for the 6.28-MeV state, as obtained in the proton-capture reaction $^{27}Al(p,\gamma)^{28}Si$ measurements (6.28 → 1.78 MeV transition). The slowing-down material is Ta. The dispersion is 0.76 keV/channel. The dashed line illustrates the instrumental line shape obtained from the 6.13-MeV background peak [from the $^{19}F(p,\alpha\gamma)^{16}O$ reaction]; $\tau(6.28)$ = 1260±110 fs.

C. The $^{27}Al(p,\gamma)^{28}Si$ reaction study

The DSA measurements were performed with a detector at angles 0° and 90° to the beam direction and a target-detector distance of 7.5 cm. The intensity of low energy γ rays and x rays was reduced by use of a 3-mm-thick lead shield between the target and the detector. The corrections for solid-angle attenuation of the observed Doppler shifts were taken into account by the use of primary γ-ray transitions at the E_p = 1317-keV resonance (Γ = 35±4 eV [18]). The accumulated charge for the γ-ray spectra varied between 0.02 and 1.0 C, depending on the strength of the resonance used.

On the basis of the proper γ-decay schemes [28, 29] and γ-ray yields high enough for DSA measurements with implanted targets, the E_p = 655-, 767-, 992-, 1213-, and 1317-keV resonances were selected. Figures 5–9 show

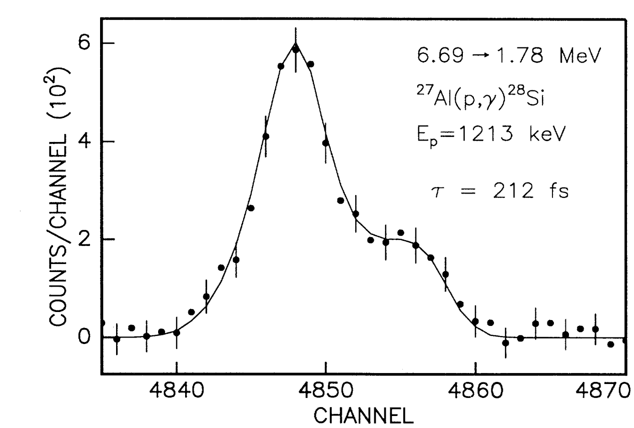

FIG. 6. As for Fig. 5, but for the 6.69-MeV state (6.69 → 1.78 MeV transition); $\tau(6.69)$ = 212±14 fs. The dispersion is 0.93 keV/channel.

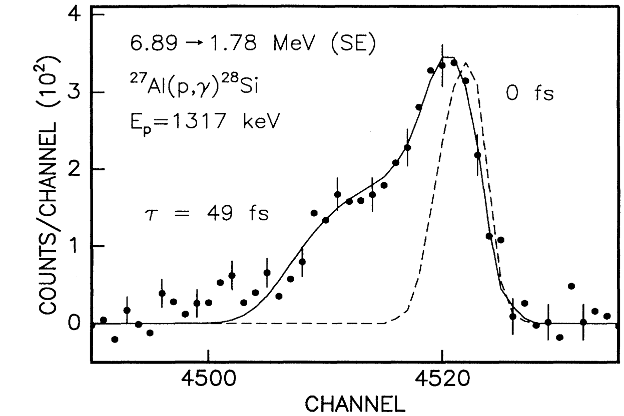

FIG. 7. As for Fig. 6, but for the 6.89-MeV state (6.89 $\rightarrow$ 1.78 MeV transition); $\tau(6.89)$ = 49$\pm$3 fs.

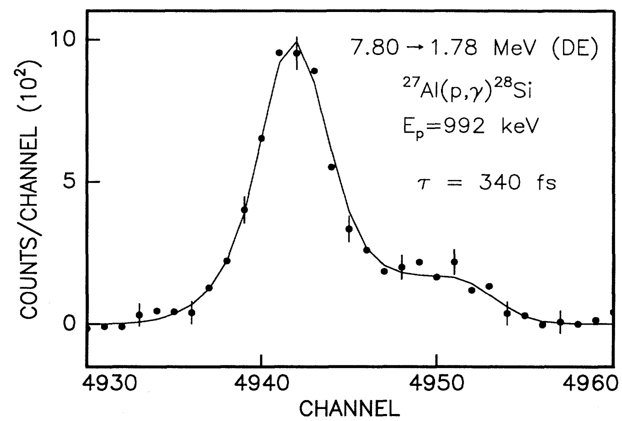

FIG. 8. As for Fig. 6, but for the 7.80-MeV state (7.80 $\rightarrow$ 1.78 MeV transition); $\tau(7.80)$ = 340$\pm$15 fs. (DE represents double-escape peak).

portions of the γ-ray spectra from the DSA measurements of the 6.28-, 6.69-, 6.89-, 7.80-, and 7.93-MeV states. The summary of the results is given in Table II. The $F(\tau)$ values shown in Table II are averages from at least two sets of measurements. The DSA analysis was carried out using the MC method in the simulations of the γ-ray line shapes and of $F(\tau)$ curves [10–16]. A χ^2 fit of the simulated and experimental 0° line shape was done in most cases. The 90° line shapes were also utilized for very short lifetimes ($\tau \leq 30$ fs), as shown in Fig. 9. The broadening of the γ-ray line shape at 90° due to the elastic scattering of the recoil atoms from the host atoms depends sensitively on the nuclear lifetime in

TABLE II. As for Table I but as obtained with the ^{27}Al$(p,\gamma)^{28}$Si reaction.

E_x (MeV)	E_p (keV)	$F(\tau)$[a] (%)	τ[b] (fs)	τ[c] (fs)
4.98	1213	47$\pm$5	51$\pm$3	51$\pm$4
6.28	1317	3.7$\pm$0.3	1260$\pm$70	1260$\pm$110
		10.9$\pm$0.8[d]	1250$\pm$100	
6.69	1213	17.7$\pm$1.5	212$\pm$9	212$\pm$14
6.89	1317	50.5$\pm$1.5	49$\pm$2	49$\pm$3
7.38	1213	93.3$\pm$1.3	4.4$\pm$0.8	4.4$\pm$1.0
7.42	1213		50$\pm$9[e]	50$\pm$9
7.80	992	12.7$\pm$1.6	343$\pm$12	340$\pm$15
	1317	15.9$\pm$1.5	330$\pm$30	
7.93	992		17$\pm$2[e]	17$\pm$2
8.26	1213	74$\pm$5	20$\pm$5	20$\pm$5
8.41	767	8$\pm$2	490^{+160}_{-60}	540$\pm$110
8.59	655	70$\pm$2	19$\pm$2	19$\pm$2
	1317	72$\pm$11	24$\pm$12	
9.32	767	98.4$\pm$1.2	1.2$\pm$0.8	1.3$\pm$0.8
	1317	89$\pm$4	4$\pm$3	
9.38	655	98.2$\pm$0.7	1.8$\pm$0.5	1.8$\pm$0.6
10.67[f]	1317	65$\pm$5	31$\pm$8	31$\pm$8

[a]Values are not corrected for feedings.
[b]Values given are corrected for the feedings and are based on the $F(\tau)$ values and on the line-shape analysis. Only statistical errors are shown.
[c]Values include the uncertainty in the experimental stopping power.
[d]Obtained with the Si backing.
[e]Based on the line-shape analysis only.
[f]The 4^+ member of the 10.67-MeV doublet.

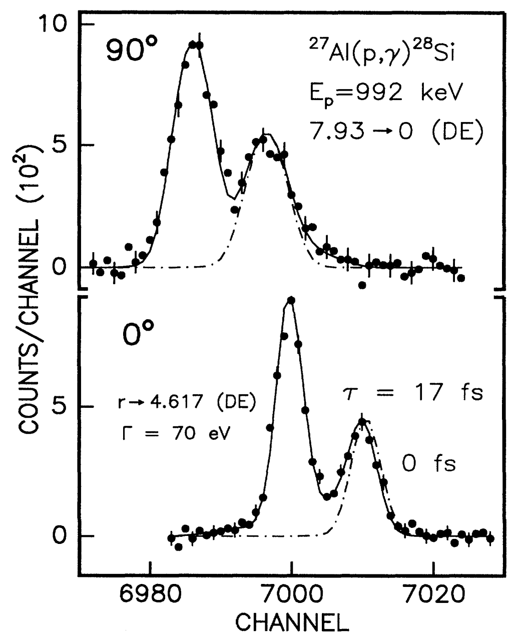

FIG. 9. As for Fig. 6, but for the 7.93-MeV state [ground state transition; $\tau(7.93)$ = 17$\pm$2 fs], and the resonant state ($r \rightarrow$ 4.62 MeV transition; Γ = 70$\pm$14 eV [18]). The solid line shows the sum of the two simulated line shapes, corresponding to the lifetimes 0 and 17 fs, for the resonance and the 7.93-MeV states, respectively. The dot-dashed line illustrates the simulation for the 7.93-MeV state with τ = 0 fs. The upper part of the figure shows the line shapes as obtained with the detector at 90° to the beam, and the lower part with the detector at 0°.

TABLE III. Lifetime measurements of the ^{28}Si levels (E_x < 8.5 MeV).

Ref.	Reaction	E_x (MeV) 4.98	6.28	6.69	6.89	7.38	7.42	7.80	7.93	8.26	8.41
This work	^{14}N(^{16}O, pn)^{28}Si	47±3	1250±150		47±8	11.5±1.5[a]	51±4		16±2		
	^{27}Al(p,γ)^{28}Si	51±4	1260±110	212±14	49±3	4.4±1.0	50±9	340±15	17±2	20±5	540±110
[30]			$1350\pm^{220}_{170}$			13±3	40±3	310±30		14±6	$280\pm^{100}_{60}$
[31]		34±12	810±490								
[32, 33]		31±6	$920\pm^{1000}_{300}$	88±12	53±6	7±4	24±4	190±30	<6		560±150
[34, 35]			1100±280	120±30	44±13	6±5	40±8				490±110
[36, 37]		$41\pm^{33}_{20}$	1500±400	100±30		6±2	39±5		12±3	8±6	580±400
[38]							40±8		9±6		
[29]				130±30	40±5	8±3	30±5	250±75	<5	26±8	
[39]		54±13	1350±400	125±30		7±4	44±10	300±75	15±10		
[40]			890±90		67±10						
[28]		81±13	990±230		27±8	<15		250±45	14±2	12±4	890±160
[41]	^{28}Si(α,α')^{28}Si				100±40						
[42]	^{25}Mg($\alpha,n\gamma$)^{28}Si	60±20	1150±130	180±40	70±20						
[43]								300±100			
[44]	^{27}Al(^{3}He, d)^{28}Si		1300±200						50±25		
[45]	^{28}Si(e,e')^{28}Si					3.5±0.9[b]	9±2[c]		21±11		
Adopted		49±3	1200±70	212±14	47±3	5.7±0.8	51±4	340±15	15.1±1.1	15±3	470±80

[a]Effective lifetime value, probably containing unknown delayed feeding (see the text). Not included in the calculation of the adopted value.

[b]The 7.38-MeV state, instead of the 7.42-MeV state, was assigned to correspond to the data of Ref. [45] (see the text).

[c]Value based on the original data of Ref. [45]. Note that cases b and c are mutually exclusive.

the region $5 \leq \tau \leq 30$ fs. The effect of the primary γ-ray emission on the initial recoil velocity was taken into account in the simulations, as is illustrated in Fig. 9. This γ-ray-induced line-shape broadening has not been considered in the previous (p,γ) measurements reported in the literature.

Corrections for delayed feedings from the resonance state were taken into account in the deduction of the lifetime values of the 4.98-, 6.89-, and the 9.32-MeV states. At the E_p = 1213-keV resonance, the feeding cascades $r \rightarrow 8.26 \rightarrow 4.98$ and $r \rightarrow 7.93 \rightarrow 4.98$, with the fractions of 14.2±0.5 % and 2.0±0.3 %, respectively, were used in the DSA analysis of the 4.98-MeV state lifetime. At the $E_p = 1317$-keV resonance, 7.1±0.5 % feeding through the 8.95-MeV state (τ=70±8 fs) was used in the analysis of the 6.89-MeV state, and 16.0±1.0 % feeding through the 10.67-MeV state (31±8 fs) in the analysis of the 9.32-MeV state. The feeding fractions are based on branching ratios reported in the literature [28, 29]. The effect of the feeding on the lifetime of the 6.28-MeV state was only 5 fs at most, and was therefore taken into account by increasing the uncertainty of the lifetime value correspondingly. The excitation energy of the 6.69-MeV 0^+ state was determined at the E_p = 1213-keV resonance, and was found to be 6690.74±0.15 keV, to be compared with the literature value of 6691.4±0.4 keV [18]. For the other states, the excitation energies were in agreement with the literature values [18].

D. Comparison with previous results

The present lifetime values obtained with the ^{14}N(^{16}O, pn)^{28}Si and the ^{27}Al(p,γ)^{28}Si reactions, are in

TABLE IV. Lifetime measurements of the ^{28}Si levels (E_x > 8.5 MeV).

Ref.	Reaction	E_x (MeV) 8.54	8.59	8.95	9.32	9.38	9.48	10.42	10.67	11.10	11.51	12.99
This work	^{14}N(^{16}O, pn)^{28}Si	16.4±1.4		70±8			7±3	38±10		15.9±1.5	13±3	23±5
	^{27}Al(p,γ)^{28}Si		19±2		1.3±0.8	1.8±0.6			31±8			
[30]			25±2		<10							
[32, 33]			<6	23±7	<5	5±3						
[34, 35]		65±12	13±4	65±12		<5		23±7				
[36, 37]		18±6	10±3		$13\pm^{7}_{13}$	<12						
[38]				$110\pm^{35}_{25}$								
[46]		18±7		$67\pm^{20}_{11}$				$28\pm^{21}_{7}$				
[47]					5±3[a]	11±5[a]						
[48]		15±3		104±8								
[29]		<5	5±2	100±8	<5	<10		27±7	22±6			
[40]		31±7		89±10	16±4			22±6				
[28]		38±14	12±3	96±19	3.1±1.5	1.4±0.5	13±6	27±11	27±6			
[49]	^{25}Mg($\alpha,n\gamma$)^{28}Si	58±12										
[50]		19±8										
[51]										<15	<30	<15
[44]	^{27}Al(^{3}He, d)^{28}Si		<25									
Adopted		16.4±1.4	19±2	70±8	2.2±1.1	1.7±0.6	8±3	27±4	26±4	15.9±1.5	13±3	23±5

[a]Reanalyzed values, corrected for delayed feedings (see the text).

a very good mutual agreement, except for the 7.38-MeV state, where the high-velocity value is considerably longer than the low-velocity value (11.5 fs vs 4.4 fs). Since short lifetimes are very sensitive to the effects of delayed feedings, this discrepancy could be due to some unknown delayed feeding in the heavy-ion reaction. Therefore, we consider the lifetime value of the 7.38-MeV state based on the (p,γ) measurements to be more reliable than the value obtained in the heavy-ion reaction. The high-velocity value is not included in the calculation of the final adopted value shown in Table III.

The previous lifetime results of the states in ^{28}Si along with our measurements are summarized in Tables III and IV. The experimental conditions of the current and previous DSA measurements are collected in Table V.

The available data in the literature is based only on DSA measurements, with the exception of the inelastic electron scattering experiment of Ref. [45], where the $E2$ radiative widths for the 7.42- and 7.93-MeV states were reported. The energy resolution of the electron spectrometer in that experiment was about 170 keV at 7.4 MeV, which was not good enough to separate the 7.38- and 7.42-MeV states (see Fig. 5 in Ref. [45]). The doublet at 7.4 MeV was originally assigned to correspond only to the 7.42-MeV state. This, however, results in a lifetime value which is shorter than the present one by a factor of 5. We suggest that the peak at 7.4 MeV had a contribution mainly from the 7.38-MeV state. If this is the case, the lifetime value of 3.5±0.9 fs for that level is obtained. This would be in excellent agreement with the present (p,γ) result.

The adopted lifetime values shown in Tables III and IV are weighted averages of current and all the previously reported values, except for the 4.98-, 6.69-, 7.42-, 7.80-, 8.54-, 8.59-, 8.95-, 11.10-, 11.51-, and 12.99-MeV states, where the current values (being the most accurate ones) were adopted. For the rest of the states, the systematic errors in previous results were assumed to be covered by the uncertainty due to the stopping power or large statistical uncertainties and all the known lifetime values were taken into account in the deduction of the weighted averages.

TABLE V. Summary of the experimental conditions in DSA measurements for lifetimes of the ^{28}Si levels studied in the present work. If the stopping power from the LSS theory [19] with the large-angle scattering corrections by Blaugrund [52] have not been used in the DSA analysis, it is marked in the footnotes.[a] The lifetime values are based on the $F(\tau)$ analysis if not stated otherwise.

Ref.	Reaction	v/c (%)	Slowing-down medium	DSA analysis
This work	^{14}N(^{16}O,pn)	2.7–3.5	Ta + implanted ^{14}N (20 μg cm^{-2})	b
	^{27}Al(p,γ)	0.13–0.19	Ta + implanted ^{27}Al (12 μg cm^{-2})	b
[30]		0.20–0.21	Evaporated Al (52 μg cm^{-2}) + Au	c
[31]		0.18–0.26	Evaporated Al (120 μg cm^{-2}) + Ta	d
[32, 33]		0.13–0.22	Evaporated Al (50 μg cm^{-2}) + Ta or Cu	e
[29]		0.14–0.25	Evaporated Al on Ta or Cu	f
[34, 35]		0.14–0.26	Evaporated Al (100 μg cm^{-2}) + Ta or Au	g
[36, 37]		0.14–0.25	Al (130 μg cm^{-2}) + Au	c
[47]		0.19	Evaporated Al (30 μg cm^{-2}) + Ta	g
[48]		0.27–0.29	Evaporated Al (100 μg cm^{-2}) + Au	g,h
[39]		0.14–0.19	Al (100 μg cm^{-2})	d
[40]		0.24	Al (45 μg cm^{-2})	g
[28]		0.13–0.19	Evaporated Al (5–30 μg cm^{-2}) + Ta	f
[41]	^{28}Si($\alpha,\alpha'\gamma$)^{28}Si	2.45–2.65	Evaporated Si (0.3 mg cm^{-2}) + Au or Mg	i, j
[42]	^{25}Mg($\alpha,n\gamma$)^{28}Si	0.70–0.78	Evaporated ^{25}Mg (114 μg cm^{-2}) + Ta	g, j
[43]		0.81	Evaporated ^{25}Mg (114 μg cm^{-2}) + Ta	g, j
[49]		0.84–0.85	Evaporated ^{25}Mg (45 μg cm^{-2}) + Ta	d
[50]		0.85	Evaporated ^{25}Mg (48 μg cm^{-2}) + Au	g, j
[51]		0.89–0.98	Self-supporting Mg (300 μg cm^{-2})	k
[44]	^{27}Al(^{3}He,$d\gamma$)^{28}Si	0.62–1.11	Evaporated Al (250 μg cm^{-2}) + Ni	g

[a]No details were given in Refs. [38] and [46].
[b]Experimental stopping power. Computer simulation of the slowing down. Doppler-broadened line-shape analysis (DBLA).
[c]An assumed 15% uncertainty in the nuclear stopping power has been taken into account.
[d]Stopping power uncertainty (20%) has been added.
[e]LSS stopping power values corrected with experimental values by Ref. [53].
[f]A 15% systematic error has been added in quadrature to the statistical error.
[g]No uncertainty in stopping power was included.
[h]Computer simulation of the slowing down using LSS stopping powers; DBLA.
[i]Experimental stopping power based on data from Refs. [54] (electronic) and [55] (nuclear).
[j] Slowing down in the target taken into account.
[k]Stopping powers from Ref. [56].

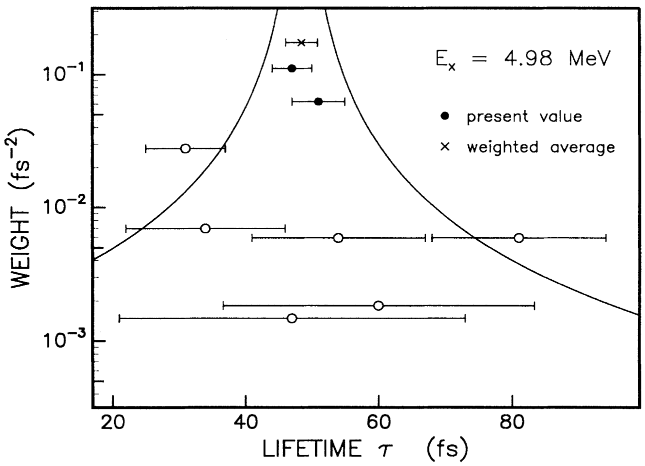

FIG. 10. A plot of the weights of lifetime measurements of the ^{28}Si 4.98-MeV state vs lifetime values. The weight of a measurement is taken as $(\Delta\tau)^{-2}$, where $\Delta\tau$ is the quoted uncertainty. If the uncertainty due to the stopping power is not included in the original paper (see Tables III–V), an uncertainty of 20% has been added in quadrature for the comparison with other values. Two contours at τ(adopted) $\pm$ 2($\Delta\tau$) are also shown.

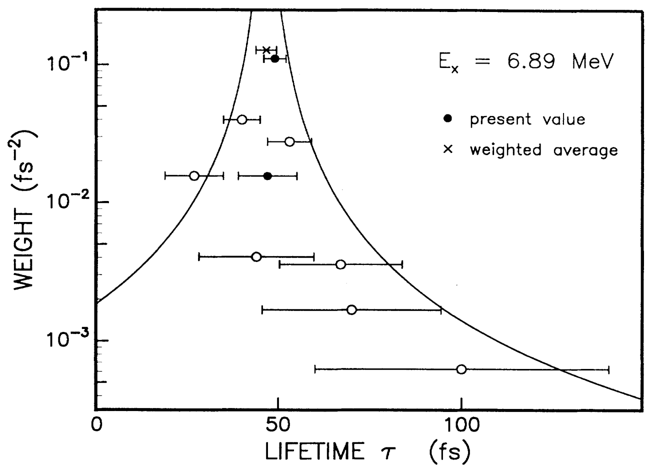

FIG. 12. As for Fig. 10, but for the 6.89-MeV state.

In the calculation of a weighted average, the weight of a measurement was taken to be $(\Delta\tau)^{-2}$, where $\Delta\tau$ is the quoted uncertainty of the lifetime measurement. The procedure is illustrated in Figs. 10–13. An uncertainty of 20% was added in quadrature in those cases where only a statistical error has been reported in the literature or where no information is available on the DSA analysis, for the comparison with the values from those measurements for which the uncertainty due to the stopping power is included. Note that even if the literature data include such an uncertainty, the values obtained without experimental stopping data can still be subject to systematic errors. For example, the effect of the unequal slowing down in the target material itself and in its backing material has been considered only in a few cases. Furthermore, the densities of the evaporated Al or Mg target layers can differ from that of bulk material. The use of the Lindhard-Scharff-Schiøtt (LSS) stopping theory [19] with the large-angle scattering corrections by Blaugrund [52] yields lifetime values which are in general shorter than the values obtained in the MC simulations. This is the reason for adopting our lifetime value for the 6.69-MeV state.

An important source of error is the neglection of the effect of the delayed feeding in almost all the previous works. Thus a complete reanalysis of the reported literature values would be desired. However, experimental conditions are not reported in such details that reanalysis would be meaningful. Only the lifetimes of the 9.32-, and 9.38-MeV states (15±2 and 12±4 fs, respectively) reported in Ref. [47] were reanalyzed. Corrections for the delayed feedings from the 10.67-MeV doublet resulted in values not in disagreement with the omnibus averages.

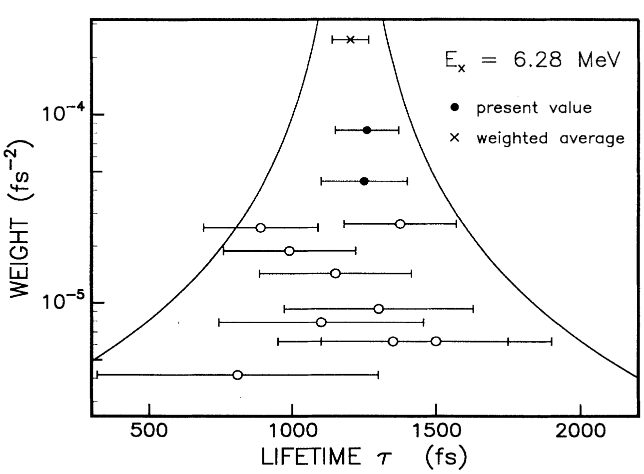

FIG. 11. As for Fig. 10, but for the 6.28-MeV state.

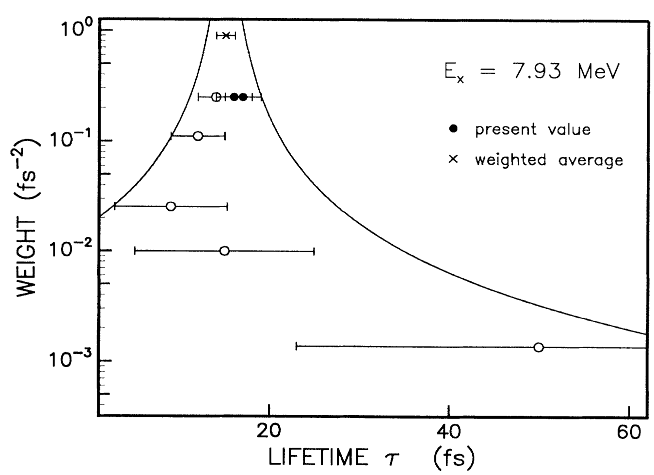

FIG. 13. As for Fig. 10, but for the 7.93-MeV state.

TABLE VI. Magnitudes of experimental matrix elements[a] for $M1$ and $E2$ transitions between positive parity states in ^{28}Si, and their comparison with shell-model calculations.

E_i (MeV)	E_f (MeV)	J_i	J_f	τ (fs)	Branching ratio (%)	$\lvert M(M1)\rvert$ (μ_N) Expt.[b]	SM	$\lvert M(E2)\rvert$ ($e\,fm^2$) Expt.[b]	SM
1.78	0	2	0	686±13[c]	100			18.3±0.2	19.9
4.62	1.78	4	2	65±5[d]	100			24.7±1.0	31.7
4.98	1.78	0	2	49±3	100			7.0±0.2	8.1
6.28	1.78	3	2	1200±70	88.2±0.3	0.056±0.002[e]	0.050	0.21±0.03[e]	0.14
	4.62		4		11.8±0.3	<0.093	0.011	<6.7	6.7
6.69	1.78	0	2	212±14	100			1.16±0.04	2.08
6.89	1.78	4	2	47±3	98.71±0.08			6.7±0.2	8.4
	4.62		4		1.29±0.08	<0.11	0.018	<5.8	7.3
7.38	0	2	0	5.7±0.8	36.3±0.5			3.4±0.2	1.2
	1.78		2		63.4±0.5	<0.42	0.008	<9.1	7.4
7.42	0	2	0	51±4	94±2			1.83±0.07	2.16
	1.78		2		6±2	<0.043	0.018	<0.92	5.20
7.80	1.78	3	2	340±15	65.9±1.1	<0.060	0.030	<1.18	0.06
	4.62		4		1.32±0.08	<0.022	0.006	<0.82	2.28
	6.28		3		32.6±1.1	<0.33	0.055	<25.9	19.2
7.93	0	2	0	15.1±1.1	83.2±1.5			2.67±0.10	0.56
	1.78		2		5.5±0.2	<0.067	0.008	<1.30	2.23
	4.62		4		4.7±0.2			5.6±0.2	3.5
	4.98		0		4.0±0.2			6.9±0.3	10.5
	6.28		3		2.4±1.2	<0.32	0.006	<22.8	4.0
8.26	0	2	0	15±3	9.0±1.5			0.80±0.10	2.30
	1.78		2		70±2	<0.22	0.025	<4.1	0.27
	4.62		4		4.0±1.0			4.1±0.7	3.3
	4.98		0		17.0±1.0			11.0±1.2	2.9
8.54	4.62	6	4	16.4±1.4	100			26.3±1.1	35.5
8.59	1.78	3	2	19±2	87.9±0.4	<0.24	0.056	<4.3	1.7
	4.62		4		4.3±1.2	<0.12	0.056	<3.6	2.9
	6.28		3		6.9±0.2	<0.34	0.081	<17.7	4.7
8.95	4.62	5	4	70±8	61±2	<0.017[f]	0.001	7.2±0.4[f]	7.3
	6.89		4		39±2	<0.025[g]	0.004	37±2[g]	30.1
9.32	1.78	3;$T=1$	2	2.2±1.1	71±2	0.55±0.14[h]	1.011	0.09±0.09[h]	0.16
	4.62		4		0.34±0.06	<0.077	0.164	<2.0	
	6.28		3		26±2	1.3±0.3[i]	3.494	10±10[i]	
	7.80		3		1.7±0.4	<0.94	1.279	<74	
9.38	0	2;$T=1$	0	1.7±0.6	3.3±0.3			1.0±0.2	1.9
	1.78		2		89.3±1.1	0.58±0.10[j]	1.105	0.8±0.5[j]	
	6.28		3		4.0±0.2	<0.47	0.868	<18.2	
	7.93		2		2.8±0.2	<1.2	0.736	<103	
9.48	0	2	0	8±3	85±2			2.4±0.4	0.74
	1.78		2		2.58±0.12	<0.045	0.011	<0.70	2.7
	4.62		4		6.4±0.3			3.5±0.6	2.0
	4.98		0		4.5±1.5			3.5±0.9	2.9
10.42	4.62	5	4	27±4	16±3	<0.138	0.071	<2.8	0.84
	6.28		3		75±3			14.3±1.1	18.6
	7.80		3		4.6±0.8			11.1±1.3	10.7
	8.95		5		4.4±0.9	<0.56	0.015	<46	11.3
10.67	1.78	4	2	26±4	7.5±0.3			0.62±0.05	2.70
	4.62		4		9.0±0.6	<0.090	0.029	<1.77	5.47
	6.28		3		24.2±0.8	<0.24	0.029	<6.5	5.0
	6.89		4		1.7±0.2	<0.079	0.047	<2.5	2.0
	7.42		2		14.8±0.5			10.7±0.8	0.47
	7.80		3		1.85±0.14	<0.124	0.004	<5.2	3.6
	7.93		2		6.9±0.2			11.3±0.9	5.8
	9.32		3;$T=1$		24.1±0.8	<1.39	0.064	<123	
11.10	4.62	6	4	15.9±1.5	100			7.6±0.4	13.8
11.51	4.62	6	4	13±3	21±2			3.3±0.4	1.8
	6.89		4		58±4			15±2	14.7

TABLE VI. *(Continued).*

E_i (MeV)	E_f (MeV)	J_i	J_f	τ (fs)	Branching ratio (%)	$\|M(M1)\|$ (μ_N) Expt.[b]	SM	$\|M(E2)\|$ ($e\,\mathrm{fm}^2$) Expt.[b]	SM
	9.16		4		21±4			49±7	23.2
12.99	8.54	7[k]	6	23±5	91±3[m]	0.61±0.07[l]	0.028	2.6±0.9[l]	10.9
	11.10		6		9±3[m]	<0.70		<44	24.6

[a]Except for lifetimes, the values are taken from Ref. [18].
[b]If the mixing ratio is not known, the experimental matrix element value (upper or lower limit) is given for a pure multipole.
[c]Taken from Ref. [18].
[d]Taken from Ref. [57].
[e]$\delta(E2/M1) = -0.14\pm0.02$.
[f]$|\delta| > 15$ or $\delta = -0.19\pm^{0.05}_{0.03}$ from Ref. [1]. Tabulated value calculated with the larger value of $|\delta|$. The smaller value of $|\delta|$ yields $|M(M1)| = (0.255\pm0.015)\mu_N$ and $|M(E2)| = 1.3\pm0.3\ e\,\mathrm{fm}^2$.
[g]$|\delta| > 25$.
[h]$\delta = -0.01\pm0.01$.
[i]$\delta = 0.2\pm0.2$.
[j]$\delta = -0.09\pm0.05$.
[k]Experimentally the spin values 5–7 are possible [51], the spin-parity assignment 7^+ is based on shell-model calculations [1].
[l]$\delta = -0.17\pm^{0.07}_{0.04}$ from Ref. [1].
[m]Taken from Ref. [1].

IV. DISCUSSION

Absolute values of the $M1$ and $E2$ matrix elements for transitions between positive parity states in ^{28}Si were deduced from the lifetimes (as measured in the current experiment and combined with previous results as described above) and the branching and mixing ratios tabulated in Ref. [18]. These experimental matrix element values are compared in Table VI with theoretical absolute values calculated from the full *sd*-shell wave functions of the USD Hamiltonian [2]. For completeness of the comparison, the first 2^+ and 4^+ states are included in Table VI, with the mean lifetimes taken from Refs. [18] and [57], respectively. When determining the correspondence between the experimental and the theoretical states, the model state with the correct spin and isospin values and nearest in energy to the experimental one was chosen. In the case of the 7.38- and 7.42-MeV 2^+ states, an inversion of the order of the states would result in a better agreement of the matrix elements.

The USD wave functions have been shown to yield a generally good accounting for spectroscopic features of *sd*-shell states when combined with the appropriate effective operators [4]. For a more detailed discussion of this "renormalization" of the $M1$ and $E2$ operators by use the effective g factors and effective charges, respectively, see, e.g., Refs. [58, 13].

Most of the transitions measured in ^{28}Si occur between states which nominally have $T = 0$. They hence have isovector transition strength only by virtue of isospin mixing. The model wave functions have rigorously good isospin and hence transitions between $T = 0$ states are purely isoscalar. As such, their $M1$ strengths are very weak because of the cancellation of the neutron and proton terms in the isoscalar $M1$ operator.

The usefulness of the lifetime data for the $M1$ matrix elements is unfortunately limited, since the mixing ratios $\delta(E2/M1)$ are measured only for seven transitions, and in two of these the mixing ratios imply only upper limits for $|M(M1)|$. Of the $\Delta T = 0$ cases, the theoretical matrix elements agree well with the experimental value only for the 6.28 → 1.78 MeV transition. The transition

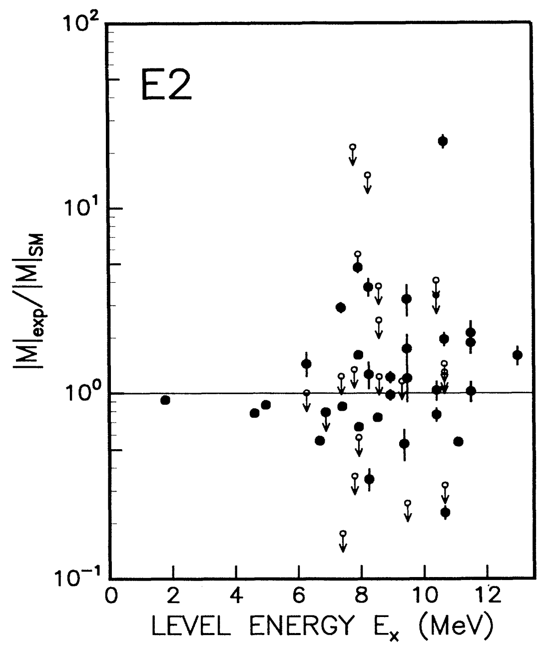

FIG. 14. Ratios of experimental to shell-model $E2$ transition matrix elements $|M(E2)|_{\mathrm{expt}}/|M(E2)|_{\mathrm{SM}}$ in ^{28}Si as a function of the initial state excitation energy (solid circles with error bars), and upper limits of these ratios [open circles with downward arrows, in cases where the mixing ratios $\delta(E2/M1)$ are unknown]. Exact agreement between experiment and theory corresponds to points which lie on the horizontal line drawn in the figure.

$12.99 \rightarrow 8.54$ MeV has an experimental matrix element which is 22 times the shell-model value. This discrepancy could be evidence of isospin mixing in the experimental wave functions at the level of a few percent. In the other $\Delta T = 0$ cases the theoretical values are well below the experimental upper limits.

The T=1, J^{π}= 3^+ analog of the ^{28}Al ground state occurs at 9.32 MeV in ^{28}Si and decays by predominantly isovector transitions to several lower-lying states. The $M1$ matrix element magnitudes range experimentally from $0.08\mu_N$ to $1.3\mu_N$. These values are about half the magnitudes of the model values, but the model values reproduce the relative strengths of the various branches quite well. The 9.38-MeV state in ^{28}Si is the $T = 1$, $J^{\pi} = 2^+$ analog of the 0.031-MeV first excited state of ^{28}Al, and decays by isovector transitions to lower states. The experimental matrix elements are again only about half of the model magnitudes. Either the model wave functions (presumably the 3^+ and 2^+, $T = 1$ wave functions in particular) do not yield enough cancellation of the $M1$ strengths, or the experimental mean lifetime values of these states are too long. Similar differences between model values and experimental values for $\Delta T = 1$ isovector $M1$ transitions have been observed previously in ^{24}Mg at about the same excitation energy [13]. It is not clear if this discrepancy could indicate a need for a model allowing isospin mixing.

The $E2$ matrix elements can be compared for 27 transitions where the mixing ratios are not needed (in addition to the seven cases mentioned above), and thus can yield more detailed information. Comparisons of the experimental and theoretical $E2$ values are illustrated in Fig. 14 where the ratios $|M(E2)|_{\rm expt}/|M(E2)|_{\rm SM}$ are plotted vs initial state excitation energy. The agreement between theory and experiment seems to be reasonably good up to about 6 MeV, above which there is considerable scatter in the ratios. The model values are systematically too large or too small. These differences could be an indication of difficulties in the shell model, i.e., the sd-shell model space is not large enough to describe the structure of the higher-lying levels. This conclusion is further supported by the evidence reported in Ref. [59] that the 12.80-MeV 6^+ state includes a $g_{9/2}$ single-particle component of 20–30 % in a nearly stretched proton configuration of $(g_{9/2}d_{5/2}^{-1})$.

In summary, the present reliable and accurate lifetime data combined with the data from literature, yield evidence for a need of multishell calculations (with the possibility of isospin mixing in the model wave functions) of the higher excited states in ^{28}Si.

ACKNOWLEDGMENTS

This work was supported by the Academy of Finland, the Hungarian Academy of Sciences, and the Hungarian National Research Fund (OTKA). Professor B. H. Wildenthal is acknowledged for providing the computer code for the calculation of the electromagnetic transition matrix elements.

[1] G. Glatz, M. Lickert, A. Burkard, T. Kern, R. Lehmann, S. Norbert, H. Röpke, J. Siefert, and B. H. Wildenthal, Z. Phys. A **324**, 173 (1986).

[2] B. H. Wildenthal, Part. Nucl. Phys. **11**, 5 (1984).

[3] B. A. Brown and B. H. Wildenthal, Nucl. Phys. **A474**, 290 (1987).

[4] B. A. Brown and B. H. Wildenthal, Annu. Rev. Nucl. Part. Sci. **38**, 29 (1988).

[5] S. Das Gupta and M. Harvey, Nucl. Phys. **A94**, 602 (1967).

[6] I. Ragnarsson, S. Åberg, and R. K. Sheline, Phys. Scr. **24**, 215 (1981).

[7] I. Ragnarsson and S. Åberg, Phys. Lett. **114B**, 387 (1982).

[8] G. C. Ball, O. Häusser, T. K. Alexander, W. G. Davies, J. S. Forster, I. V. Mitchell, J. R. Beene, D. Horn, and W. McLatchie, Nucl. Phys. **A349**, 271 (1980).

[9] M. Carchidi and B. H. Wildenthal, Phys. Rev. C **37**, 1681 (1988).

[10] J. Keinonen, in *Capture γ-Ray Spectroscopy and Related Topics—1984 (Holiday Inn-World's Fair, Knoxville, Tennessee)*, Proceedings of the Fifth International Symposium on Capture γ-Ray Spectroscopy and Related Topics, AIP Conf. Proc. No. 125, edited by S. Raman (AIP, New York, 1985) p. 557.

[11] P. Tikkanen, J. Keinonen, V. Karttunen, and A. Kuronen, Nucl. Phys. **A456**, 337 (1986).

[12] P. Tikkanen, J. Keinonen, R. Lappalainen, and B. H. Wildenthal, Phys. Rev. C **36**, 32 (1987).

[13] J. Keinonen, P. Tikkanen, A. Kuronen, Á. Z. Kiss, E. Somorjai, and B. H. Wildenthal, Nucl. Phys. **A493**, 124 (1989).

[14] P. Tikkanen, J. Keinonen, K. Arstila, A. Kuronen, and B. H. Wildenthal, Phys. Rev. C **42**, 581 (1990).

[15] P. Tikkanen, J. Keinonen, A. Kuronen, Á. Z. Kiss, E. Koltay, É. Pintye, and B. H. Wildenthal, Nucl. Phys. **A517**, 176 (1990).

[16] P. Tikkanen, J. Keinonen, A. Kangasmäki, Zs. Fülöp, Á. Z. Kiss, and E. Somorjai, Phys. Rev. C **43**, 2162 (1991).

[17] P. M. Endt and C. van der Leun, Nucl. Phys. **A310**, 1 (1978).

[18] P. M. Endt, Nucl. Phys. **A521**, 1 (1990).

[19] J. Lindhard, M. Scharff, and H. E. Schiøtt, Mat. Fys. Medd. Dan. Vid. Selsk. **33** (1963).

[20] J. Keinonen, V. Karttunen, J. Räisänen, F.-J. Bergmeister, A. Luukkainen, and P. Tikkanen, Phys. Rev. B **34**, 8981 (1986).

[21] A. Kehrel, J. Keinonen, P. Haussalo, K. P. Lieb, and M. Uhrmacher, Rad. Eff. Def. **118**, 297 (1991).

[22] W. H. Trzaska, Nucl. Instrum. Methods A **297**, 223 (1990).

[23] J. F. Ziegler, J. P. Biersack, and U. Littmark, in *The Stopping and Range of Ions in Solids*, edited by J. F. Ziegler (Pergamon, New York, 1985), Vol. 1.

[24] A. Luukkainen, J. Keinonen, and M. Erola, Phys. Rev. B **32**, 4814 (1985).

[25] A. Anttila, M. Bister, A. Luukkainen, Á. Z. Kiss, and E. Somorjai, Nucl. Phys. **A385**, 194 (1982).

[26] R. Paltemaa, J. Räisänen, M. Hautala, and A. Anttila,

Nucl. Instrum. Methods **218**, 785 (1983).
[27] J. Keinonen, K. Arstila, and P. Tikkanen, Appl. Phys. Lett. **60**, 228 (1992).
[28] P. M. Endt, C. Alderliesten, F. Zijderhand, A. A. Wolters, and A. G. M. van Hees, Nucl. Phys. **A510**, 209 (1990).
[29] M. A. Meyer, I. Venter, and D. Reitmann, Nucl. Phys. **A250**, 235 (1975).
[30] E. F. Gibson, K. Battleson, and D. K. McDaniels, Phys. Rev. **172**, 1004 (1968).
[31] M. Bister, A. Anttila, and J. Räsänen, Can. J. Phys. **47**, 2539 (1969).
[32] M. A. Meyer and N. S. Wolmarans, Nucl. Phys. **A136**, 663 (1969).
[33] M. A. Meyer, N. S. Wolmarans, and D. Reitmann, Nucl. Phys. **A144**, 261 (1970).
[34] M. M. Aléonard, D. Castera, P. Hubert, F. Leccia, P. Mennrath, and J. P. Thibaud, Nucl. Phys. **A146**, 90 (1970).
[35] J. Dalmas, F. Leccia, and M. M. Aléonard, Phys. Rev. C **9**, 2200 (1974).
[36] F. C. P. Huang and D. K. McDaniels, Phys. Rev. C **2**, 1342 (1970).
[37] F. C. P. Huang, E. F. Gibson, and D. K. McDaniels, Phys. Rev. C **3**, 1222 (1971).
[38] J.-P. Gonidec, C. Miehé, and G. Walter, C.R. Acad. Sci. **272B**, 1385 (1971).
[39] J. Dalmas and G. Y. Petit, Can. J. Phys. **56**, 917 (1978).
[40] V. K. Mittal, D. K. Avasthi, and I. M. Govil, Indian J. Pure Appl. Phys. **21**, 546 (1983).
[41] S. W. Robinson and R. D. Bent, Phys. Rev. **168**, 1266 (1968).
[42] A. E. Litherland, P. J. M. Smulders, and T. K. Alexander, Can. J. Phys. **47**, 639 (1969).
[43] T. K. Alexander, C. Broude, A. J. Ferguson, J. A. Kuehner, A. E. Litherland, R. W. Ollerhead, and P. J. M. Smulders, Can. J. Phys. **47**, 651 (1969).
[44] J. H. Anderson and R. C. Ritter, Nucl. Phys. **A128**, 305 (1969).
[45] P. Strehl, Z. Phys. **234**, 416 (1970).
[46] G. F. Neal and S. T. Lam, Bull. Am. Phys. Soc. **19**, 74 (1974).
[47] A. Anttila, J. Keinonen, and M. Bister, Nucl. Instrum. Methods **124**, 605 (1975).
[48] G. G. Frank, B. C. Robertson, and W. McLatchie, Nucl. Phys. **A255**, 351 (1975).
[49] S. T. Lam, A. E. Litherland, and T. K. Alexander, Can. J. Phys. **47**, 1371 (1969).
[50] W. R. Dixon, R. S. Storey, A. L. Carter, and H. L. Pai, Can. J. Phys. **53**, 1505 (1975).
[51] F. Glatz, J. Siefert, P. Betz, F. Bitterwolf, A. Burkard, F. Heidinger, Th. Kern, R. Lehmann, S. Norbert, and H. Röpke, Z. Phys. A **303**, 239 (1981).
[52] A. E. Blaugrund, Nucl. Phys. **88**, 501 (1966).
[53] J. H. Ormrod, J. R. McDonald, and H. E. Duckworth, Can. J. Phys. **43**, 275 (1965).
[54] L. C. Northcliffe, Annu. Rev. Nucl. Sci. **13**, 67 (1963).
[55] D. I. Porat and K. Ramavataram, Proc. Phys. Soc. London **78**, 1135 (1961).
[56] L. C. Northcliffe and R. F. Schilling, Nucl. Data Tables **A7**, 233 (1970).
[57] J. Keinonen, A. Luukkainen, A. Anttila, and M. Erola, Nucl. Instrum. Methods **216**, 249 (1983).
[58] M. C. Etchegoyen, A. Etchegoyen, B. H. Wildenthal, B. A. Brown, and J. Keinonen, Phys. Rev. C **38**, 1382 (1988).
[59] S. Kubano, K. Morita, M. H. Tanaka, A. Sakaguchi, M. Sugitani, and S. Kato, Phys. Rev. C **33**, 1524 (1986).